npj Biofilms and Microbiomes

https://doi.org/10.1038/s41522-026-00926-8

Article in Press

The ppGpp-HpaR1-*gum* regulatory pathway modulates exopolysaccharides production in *Xanthomonas campestris* pv. *campestris*

Received: 26 August 2025

Accepted: 24 January 2026

Cite this article as: Bai, K., Xu, X., Yu, C. *et al.* The ppGpp-HpaR1-*gum* regulatory pathway modulates exopolysaccharides production in *Xanthomonas campestris* pv. *campestris*. *npj Biofilms Microbiomes* (2026). https://doi.org/10.1038/s41522-026-00926-8

Kaihong Bai, Xiaoli Xu, Chengxuan Yu, Huayu Yan, Miaomiao Lyu, Na Jiang, Jianqiang Li, Jingnan Zhang, Zhenlong Wang & Laixin Luo

Title

The ppGpp-HpaR1-*gum* regulatory pathway modulates exopolysaccharides production in *Xanthomonas campestris* pv. *campestris*

Authors

Kaihong Bai[1,2†]*, Xiaoli Xu[2†], Chengxuan Yu[2], Huayu Yan[2], Miaomiao Lyu[1], Na Jiang[2], Jianqiang Li[2], Jingnan Zhang[1], Zhenlong Wang[1], Laixin Luo[2]

[†]Kaihong Bai and Xiaoli Xu contributed equally to this work.

***Corresponding author**

Kaihong Bai

Email: bkh0616@zzu.edu.cn

Affiliations

[1]School of Life Sciences, Zhengzhou University, Zhengzhou, Henan 450001, China

[2]Department of Plant Pathology, China Agricultural University, Beijing Key Laboratory of Seed Disease Testing and Control, MOA Key Lab of Pest Monitoring and Green Management, Beijing, 100193, China.

Running title

Regulation of ppGpp on EPS production

Abstract

Exopolysaccharides (EPS) are critical components of the biofilm matrix, and ppGpp has been demonstrated to positively influence biofilm formation. Here, we elucidate the underlying mechanism by which ppGpp regulates EPS production by facilitating HpaR1 to modulate the expression of the *gum* cluster in the phytopathogen *Xanthomonas campestris* pv. *campestris* (Xcc). ppGpp affected the yield of EPS without influencing its primary or advanced structure, as confirmed by Fourier transform infrared spectroscopy and scanning electron microscopy. Expression of the *gum* cluster, which governs EPS biosynthesis in Xcc, was down-regulated in the ppGpp-deficient mutant (Δ*relA*Δ*spoT*) compared to the wild type (WT). Comparison of EPS production between knock-out mutants of the *gum* cluster and ppGpp-deficient mutant revealed that the *gum* cluster was a key determinant of EPS production, with ppGpp acting upstream of the *gum* cluster. Transcriptomic and qPCR analyses indicated that ppGpp modulated global transcription in Xcc, positively regulating expression of *hpaR1*, which encodes the transcription factor for the *gum* cluster. This regulatory role was further substantiated by electrophoretic mobility shift assays, which showed that ppGpp enhanced the DNA-binding activity of HpaR1. Furthermore, genetic complementation with *hpaR1* restored EPS production, confirming its functional role in this regulatory pathway. In summary, these findings provide novel insights into the molecular mechanisms linking ppGpp signaling to EPS production in *X. campestris* pv. *campestris*.

Keywords

ppGpp, exopolysaccharides, *gum* cluster, HpaR1, *Xanthomonas campestris* pv. *campestris*

Introduction

Exopolysaccharides (EPS) play a critical role in the composition of bacterial biofilms, facilitating attachment, environmental adaptation, and stress tolerance[1]. In pathogenic bacteria, EPS protects against host defense response and enhances virulence[2].

Xanthomonas campestris pv. *campestris* (Xcc), a Gram-negative plant pathogenic bacterium belonging to Gammaproteobacteria, is a significant seed-borne pathogen[3-5]. As the causal agent of black rot disease in crucifers, Xcc causes significant economic losses worldwide. The bacteria invade the vascular system of cruciferous vegetables, synthesizing a substantial amount of EPS that occlude xylem vessels, leading to tissue necrosis and ultimately forming "V" shaped lesions on the leaves[6]. Moreover, the EPS contributes to virulence by suppressing host callose deposition and inhibiting the innate immune responses triggered by the diffusible signal factor (DSF)[7,8].

Xcc EPS, termed xanthan gum, consists of pentameric repeat units[9]. Its biosynthesis is governed by the *gum* operon (*gumB* to *gumM*), transcribed as a single unit from the *gumB* promoter. The *gumB* gene encodes an outer membrane polysaccharide export protein[10,11]. Furthermore, the GumD has glucose-1-phosphotransferase activity, which catalyzes the addition of glucose 1-phosphate to the polyisoprenol phosphate carrier. This reversible reaction represents the initial stage in the biosynthesis of lipid-linked intermediates for xanthan synthesis in Xcc[12]. The production of xanthan is under a multi-tiered regulatory network. It is coordinately and positively regulated by the regulation of pathogenicity factors (*rpf*) gene cluster through DSF-mediated quorum sensing (QS)[13-15]. Additionally, Clp, a global regulator in the QS pathway, is a c-di-GMP effector and it positively regulates xanthan production[16-18]. Several transcription factors also influence EPS yield. For instance, HpaR1, a transcriptional regulator of the *gum* gene cluster, enhances *gum* operon transcription and thereby increases EPS

production[19].

The alarmone ppGpp is a global regulator and plays an important role in bacterial survival by triggering the stringent response when exposed to environmental stress. The enzymes responsible for ppGpp synthesis and hydrolysis can be divided into long RelA/SpoT homologue (RSH) proteins, small alarmone synthetases (SAS), and small alarmone hydrolases (SAH)[20]. The cellular repertoire of these enzymes varies greatly among different bacterial lineages[21]. The Betaproteobacteria and Gammaproteobacteria classes typically contain two RSHs (RelA and SpoT), whereas other bacterial classifications contain a single RSH enzyme (Rel)[22,23]. RSH and SAS enzymes catalyze the key step in ppGpp synthesis by transferring the pyrophosphate group from ATP to the 3' -hydroxyl group of GDP[24]. ppGpp exerts a significant influence on a variety of cellular processes, including transcription, translation, replication, and nutrient metabolism[25,26] and plays an important role in regulating the virulence of plant pathogenic bacteria including *Xanthomonas campestris* pv. *campestris*, *Xanthomonas citri* subsp. *citri*, *Pectobacterium atrosepticum* (previous synonym: *Erwinia carotovora* subsp. *atroseptica*), *Clavibacter michiganensis*, and *Erwinia amylovora*[27-32]. It also promotes biofilm formation in various bacterial species, including *Helicobacter pylori*, *Mycobacterium smegmatis*, *Streptococcus mutans*, *Pseudomonas aeruginosa*, and *Listeria monocytogenes*[33-37]. Supporting its role in EPS production, our previous transcriptome data revealed that ppGpp affects the expression of EPS-related genes in *C. michiganensis*, and its deficiency reduces EPS yield in both *C. michiganensis* and Xcc[27,28,32]. However, the precise mechanistic role of ppGpp in EPS production remains poorly understood.

Our previous report confirmed that double-deletion mutant of genes *relA* and *spoT* (Δ*relA*Δ*spoT*) is ppGpp-deficient mutant which reduced the EPS production (as measured by colony diameter), biofilm formation, and pathogenicity in Xcc[28]. Here, we further quantified the EPS yield via absolute ethanol deposition and

investigated the primary and advanced structures of EPS in wild-type (WT) and ppGpp-deficient mutant. We demonstrated that ppGpp acted upstream of the *gum* cluster, enhancing its transcription via the regulator HpaR1, thereby modulating EPS production. To the best of our knowledge, this is the first study to explore the mechanism by which ppGpp regulates EPS production.

Results

ppGpp strongly affects EPS production in Xcc

EPS production was investigated by culturing Xcc on NYGA plates amended with 2% glucose. The results showed that the diameters of the colonies of the Δ*relA*Δ*spoT* and pL3-Δ*relA*Δ*spoT,* which were ppGpp-deficient mutant and ppGpp-deficient mutant with an empty vector, were both 11.50 ± 0.00 mm, exhibited a significant decrease compared to 17.00 ± 0.50 mm and 17.05 ± 0.50 mm of the WT and pL3-WT, respectively (Figure 1A and B). It is noteworthy that the colony diameters of Δ*relA*, pL3-Δ*relA*, Δ*relA*(*relA*) and Δ*relA*Δ*spoT*(*spoT*) were also smaller than those of WT and pL3-WT (Figure 1B). Furthermore, the EPS was extracted using absolute ethanol and subsequently quantified. The EPS yields of Δ*relA*Δ*spoT* (4.27 ± 0.29 mg) and pL3-Δ*relA*Δ*spoT* (4.33 ± 0.12 mg) were significantly lower than those of WT (6.03 ± 0.15 mg) and pL3-WT (6.07 ± 0.21 mg, consistent with the aforementioned results concerning the colony diameter (Figure 1C). These results demonstrated that the ppGpp-deficient mutant produced less EPS.

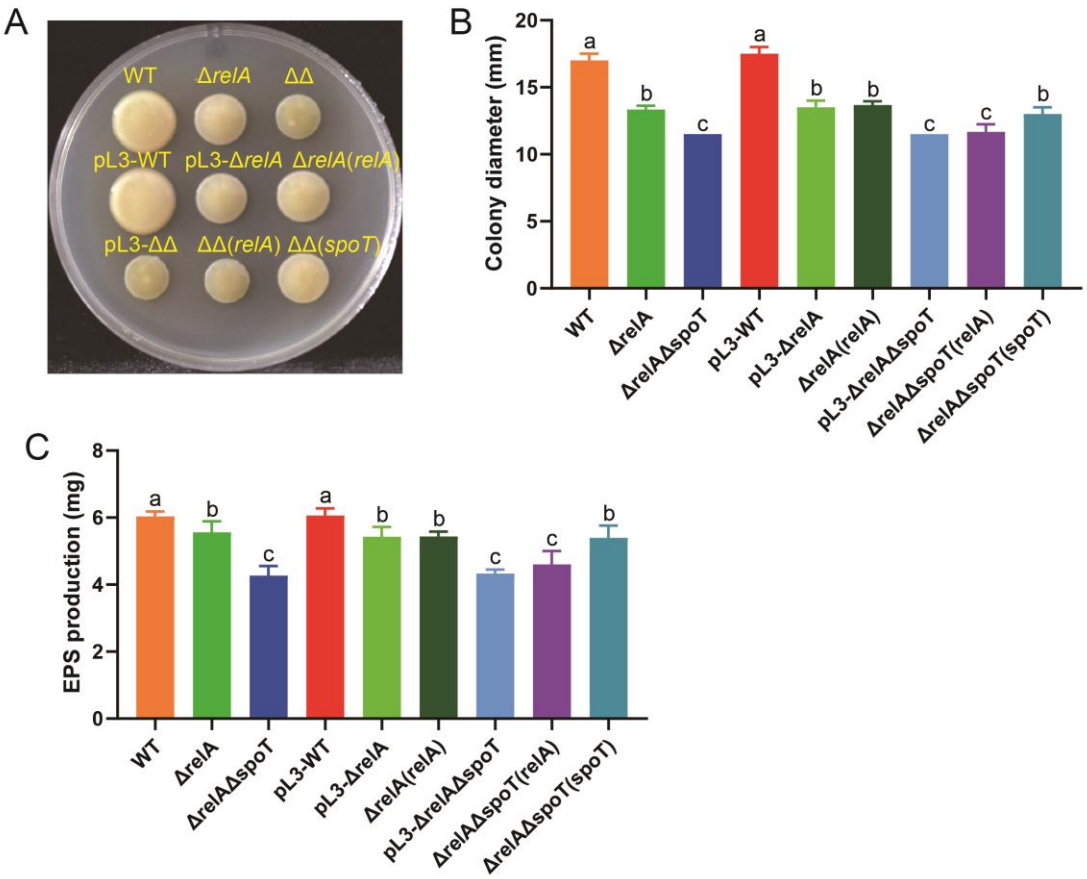

Figure 1 Effect of ppGpp on EPS production. A, The colonies were produced during the EPS secretion assay on NYGA containing 2% glucose. B, The colony diameter data were obtained from the EPS assay. C, EPS yield was determined by absolute ethanol deposition method. Bars correspond to one standard deviation (SD) from the mean (n = 3), while different letters above columns indicate significant differences ($P< 0.05$) among samples in different mutants according to a one-way ANOVA in conjunction with the Duncan's multiple range test.

ppGpp has no effect on the primary and advanced structures of EPS

The functional groups of EPS were detected using the Fourier transform infrared spectrometer (FTIR). The FTIR characteristic peaks were assigned according to the information from previous research[38-41]. The FTIR spectra of the EPS from all strains exhibited a high degree of similarity (Figure 2A). The following characteristic

peaks were identified: O-H stretching vibrations at 3276 cm^{-1}, CH_2 asymmetric stretching vibration of aliphatic chains at 2932 cm^{-1}, amide I and amide II groups at 1638 and 1548 cm^{-1}, COOH and P-O-H groups at 1562 cm^{-1} and 1402 cm^{-1}, and carboxylic acids C=O stretching at 1242 cm^{-1}. Furthermore, bands at 1030 cm^{-1} were assigned to the C-O-H and C-O bonding of glucose in pyranose form[42]. The results indicated that the EPS of all strains had identical types and quantities of functional group.

Scanning electron microscopy (SEM) further characterized the EPS. The EPS of WT and Δ*relA*Δ*spoT* exhibited a cheese-like porous surface at 50× magnification (Figure S1 A and B), and these surfaces were irregular in sheet structure with slightly rough and wrinkled surfaces at 500× magnification (Figure S1C and D). The EPS manifested as a spherical structure at 5000× magnification (Figure S1E and F), a finding that aligned with the previous report[43]. A quantitative analysis of the samples revealed that the spherical lumps of Δ*relA*Δ*spoT* EPS exhibited a significant increase in size when observed at 10000× magnification in comparison to those of WT (Figure 2B).

When considered as a whole, the FTIR and SEM results indicated that ppGpp did not affect the primary or advanced structure of EPS, despite the observed size differences between the WT and the ppGpp-deficient mutant (Δ*relA*Δ*spoT*). We proposed that the effect of ppGpp on EPS yield was not mediated through alterations in the function of synthesis enzymes and metabolites, but rather through the level of gene regulation.

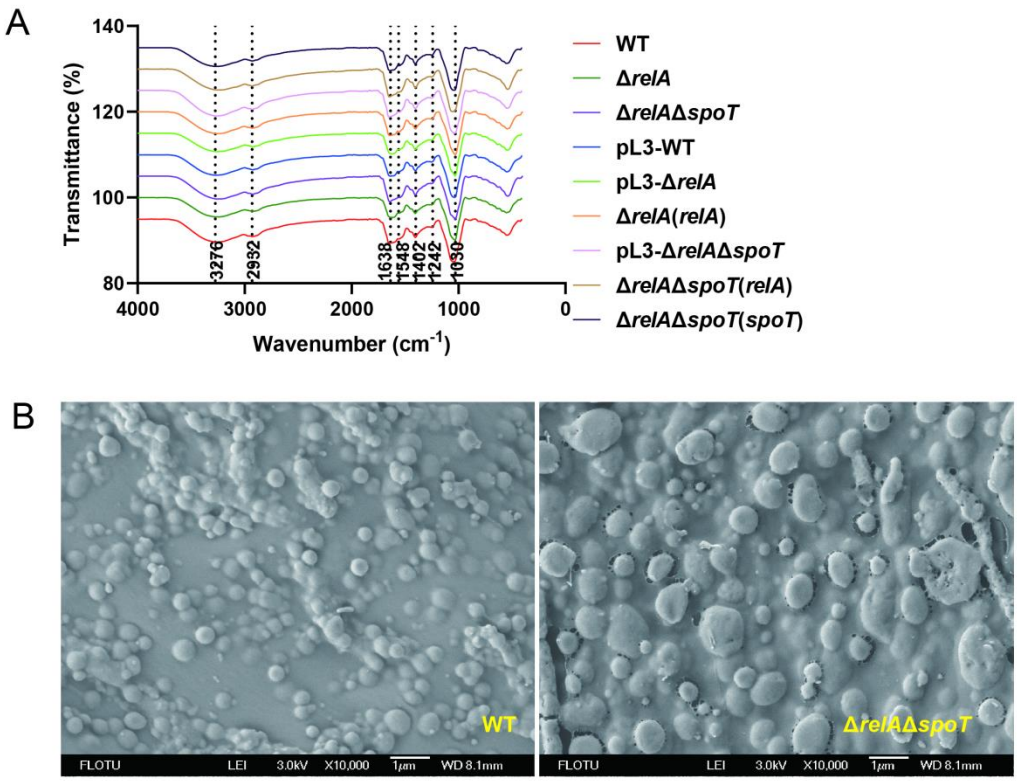

Figure 2 Effect of ppGpp on EPS characteristics. A, The EPS primary structure of WT, Δ*relA*, Δ*relA*Δ*spoT*, pL3-WT, pL3-Δ*relA*, Δ*relA*(*relA*), pL3-Δ*relA*Δ*spoT*, Δ*relA*Δ*spoT*(*relA*), and Δ*relA*Δ*spoT*(*spoT*) detected by Fourier transform infrared spectrometry (FTIR). The functional groups of EPS were labeled. B, The EPS advanced structure of WT and Δ*relA*Δ*spoT* determined by scanning electron microscope (SEM). Bar indicates 1 μm.

ppGpp acts upstream of the *gum* cluster to regulate EPS production

The location of the *gum* cluster on the genome is illustrated in Figure 3A, and it has been demonstrated to be responsible for EPS production. The expression levels of *gumB- gumM* were detected in WT, Δ*relA* and Δ*relA*Δ*spoT*, respectively. The results showed that the expression of *gumB-gumM* was significantly down-regulated in the Δ*relA* and Δ*relA*Δ*spoT*, with the lowest expression observed in Δ*relA*Δ*spoT* strain (Figure 3B).

These results indicated that ppGpp could positively regulate the expression of the *gum* cluster.

It was reported that the *gum* cluster is a single operon[10]. GumD was the first enzyme to function in the *gum* cluster in the step of EPS production[12]. We selected the gene *gumD* to construct its knock-out mutants and complementary transformants in WT and Δ*relA*Δ*spoT* strains, respectively. The EPS of all strains was extracted by absolute ethanol deposition method and subsequently analyzed. The results demonstrated that EPS yields in Δ*gumD* (3.42 ± 0.13 mg) and Δ*relA*Δ*spoT*Δ*gumD* (3.10 ± 0.17 mg) were significantly reduced compared to both Δ*relA*Δ*spoT* (4.38 ± 0.13 mg) and the complemented strain Δ*relA*Δ*spoT*Δ*gumD*(*gumD*) (4.31 ± 0.12 mg). Notably, the EPS yield of all the above derived strains was significantly lower than that of WT (5.46 ± 0.22 mg) and Δ*gumD*(*gumD*) (5.43 ± 0.28 mg) (Figure 3C). These results suggested that the *gum* cluster had a greater impact on EPS production than ppGpp in this regulatory pathway. Since ppGpp modulated the expression of the *gum* cluster, we concluded that ppGpp functioned upstream of the *gum* cluster, controlling its expression to ultimately affect EPS yield. Based on these findings, we proposed that ppGpp likely regulated the transcription of the *gum* cluster.

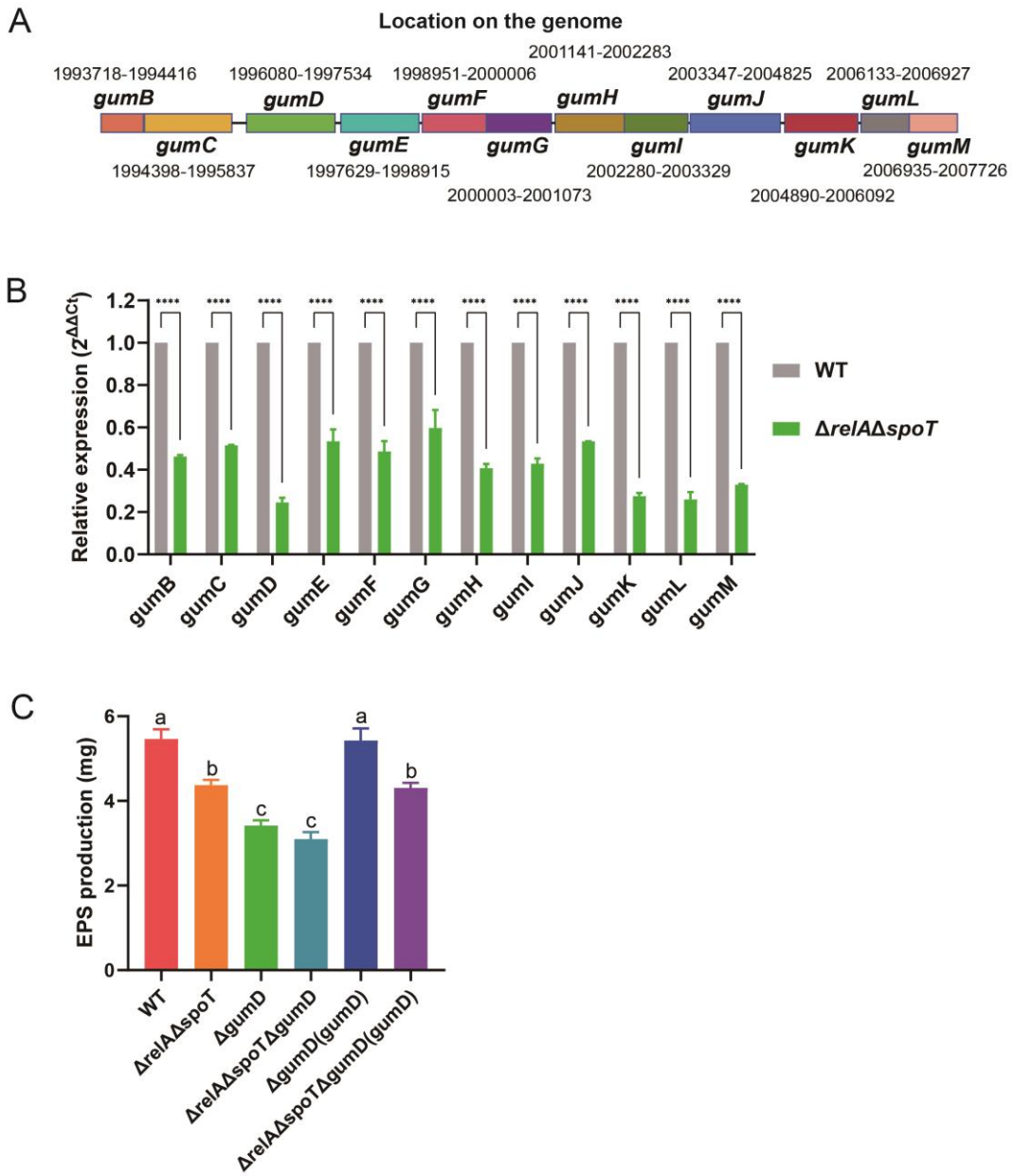

Figure 3 ppGpp regulates *gum* gene cluster expression and EPS production. A, The location on the genome of the *gum* cluster (*gumB*- *gumM*) in Xcc 8004. B, The gene expression of *gum* cluster in WT and Δ*relA*Δ*spoT*. Bars correspond to one standard deviation (SD) from the mean (n = 3), while asterisks indicate significant differences ($P< 0.05$) determined by a one-way ANOVA in conjunction with the Dunnett's multiple comparison test in comparison with WT. ****, $P< 0.0001$. C, EPS yield of WT, Δ*relA*Δ*spoT*, Δ*gumD*, Δ*relA*Δ*spoT*Δ*gumD*,

Δ*gumD*(*gumD*), and Δ*relA*Δ*spoT*Δ*gumD*(*gumD*). Bars correspond to one standard deviation (SD) from the mean (n = 3), while different letters above columns indicate significant differences ($P< 0.05$) among samples in different mutants according to a one-way ANOVA in conjunction with the Duncan's multiple range test.

ppGpp improves the function of transcription factor HpaR1

To investigate ppGpp-mediated transcriptional regulation, we performed RNA-seq analysis of bacterial cultures grown in NYGB medium supplemented with 4% glucose. The data produced consisted of a total of 162561456 raw reads (PRJNA1011498, SRA, NCBI), which yielded 161017708 clean reads with 22821501790 clean bases after low-quality reads had been removed by filtering to produce samples having Q20 and Q30 values greater than 98.56% and 95.66%, respectively (Table S1). The expressed genes were counted in various databases, yielding 4199 genes (99.08%), 2856 genes (67.39%), 3606 genes (85.09%), 3464 genes (81.74%), 3101 genes (73.17%) and 2268 genes (53.52%) annotated in NR, Swiss-Prot, Pfam, COG, GO and KEGG databases, respectively (Figure S2).

A total of 4173 genes were identified by aligning the RNA-seq data to the reference genome (RefSeq assembly: GCF_000012105.1), and subsequent cluster analysis was conducted on these genes. The samples from WT (designated as W1, W2, and W3) were grouped into a single clade, while the Δ*relA*Δ*spoT* samples (designated as D1, D2, and D3) were grouped in another clade (Figure 4A). The results indicated that the expression profiles of WT and Δ*relA*Δ*spoT* were distinct, and ppGpp could affect global gene expression. Differential gene expression analysis confirmed significant down-regulation of the *gum* cluster in Δ*relA*Δ*spoT*, consistent with qPCR results (Figure 4B). Among the 391 predicted transcription factor genes, 368 genes were expressed (Data S1). Cluster analysis indicated significant differences in their expression profiles between WT

and Δ*relA*Δ*spoT* (Figure 5A). These results indicated that ppGpp could affect transcription in Xcc.

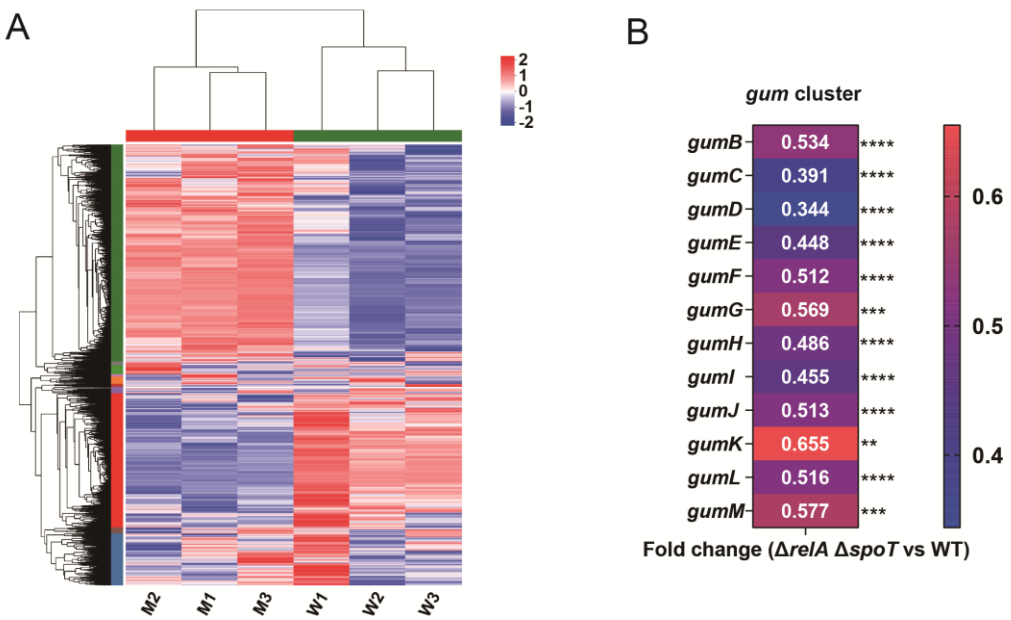

Figure 4 Transcriptomic analysis reveals the effect of ppGpp on gene expression levels including the *gum* cluster in *Xanthomonas campestris* pv. *campestris*. A, The heatmap depicting the average expression levels of the 4173 genes identified through RNA-seq alignment to the reference genome (RefSeq assembly: GCF_000012105.1) was generated to visualize the similarity between different treatments. M indicates double mutant (Δ*relA*Δ*spoT,* ppGpp-deficient mutant), while W indicates wild-type (WT). The numbers 1, 2, and 3 indicate three independent biological replicates. Expression values are presented as $\log_{10}$(TPM+1) and are row-normalized (Z-score). Blue to red colors reflect gene expression levels (values from -2 to 2). B, The fold change of the *gum* cluster (*gumB-gumM*) in Δ*relA*Δ*spoT* compared with wild-type (WT). The asterisks indicate significant differences ($P< 0.05$) determined by a one-way ANOVA in conjunction with the Dunnett's multiple comparison test in comparison with WT. **, $P< 0.01$; ***, $P< 0.001$; ****, $P< 0.0001$.

Further analysis of transcription factor expression results showed that *hpaR1*, the transcription factor of

gum cluster[19], was significantly down-regulated in Δ*relA*Δ*spoT* (Figure 5B). Electrophoretic mobility shift assay (EMSA) was performed to verify HpaR1's binding to both the *gum* cluster and its own promoter. When FAM-labeled promoter DNA of the *gum* cluster and *hpaR1* was incubated with increasing concentrations of HpaR1 protein, we observed increased binding complex formation and deeper band intensity. Control reactions containing only GST protein showed no binding complex. Furthermore, adding unlabeled probes led to increased free oligonucleotides and reduced complex band intensity, confirming competitive binding (Figure 5C and D). These results indicated that HpaR1 could specifically bind the promoters of the *gum* cluster and its own, which was consistent with the previous reports[19,44].

The expression levels of *hpaR1* were detected by qPCR in different strains, including WT, Δ*hpaR1*, Δ*relA*Δ*spoT*, WT with overexpressed *hpaR1* (WT(*hpaR1*)), complementation of *hpaR1* in Δ*hpaR1* (Δ*hpaR1*(*hpaR1*)), and Δ*relA*Δ*spoT* with overexpressed *hpaR1* (Δ*relA*Δ*spoT*(*hpaR1*)). The results demonstrated that *hpaR1* was down-regulated in Δ*relA*Δ*spoT*, which was consistent with the RNA-seq data. Notably, overexpression or complementation of *hpaR1* in WT, Δ*hpaR1*, and Δ*relA*Δ*spoT* backgrounds showed significantly higher *hpaR1* expression levels than that of WT. The *hpaR1* expression was abolished in the Δ*hpaR1* mutant and was significantly reduced in the Δ*relA*Δ*spoT* mutant compared to WT. Intriguingly, the expression level of *hpaR1* in strains of Δ*hpaR1*(*hpaR1*) and Δ*relA*Δ*spoT*(*hpaR1*) was significantly higher than that of WT(*hpaR1*) (Figure 5E). We speculated that the high expression of *hpaR1* in the background strain (WT) inhibited its own expression, resulting in the lowest expression level in WT(*hpaR1*). This finding, along with previous reports of HpaR1's autoregulatory capacity[44], suggested stronger feedback inhibition in WT(*hpaR1*) than in Δ*relA*Δ*spoT*(*hpaR1*), providing additional evidence that ppGpp enhanced HpaR1 function.

We further demonstrated the effect of ppGpp on HpaR1 by supplementing the EMSA reaction system with

ppGpp at concentrations of 1, 10, 100, and 500 μM. The addition of ppGpp enhanced the binding affinity of HpaR1 to both the *gum* promoter and its own promoter (Figure 5F and G), indicating that ppGpp improved the function of HpaR1. Interestingly, the enhancing effect of ppGpp on HpaR1 exhibited a concentration-dependent biphasic response: it initially increased and then decreased with rising ppGpp concentrations. Nevertheless, even at 500 μM ppGpp, where the enhancement was weaker, the DNA-binding activity of HpaR1 toward both target promoters remained stronger than that observed in the absence of ppGpp.

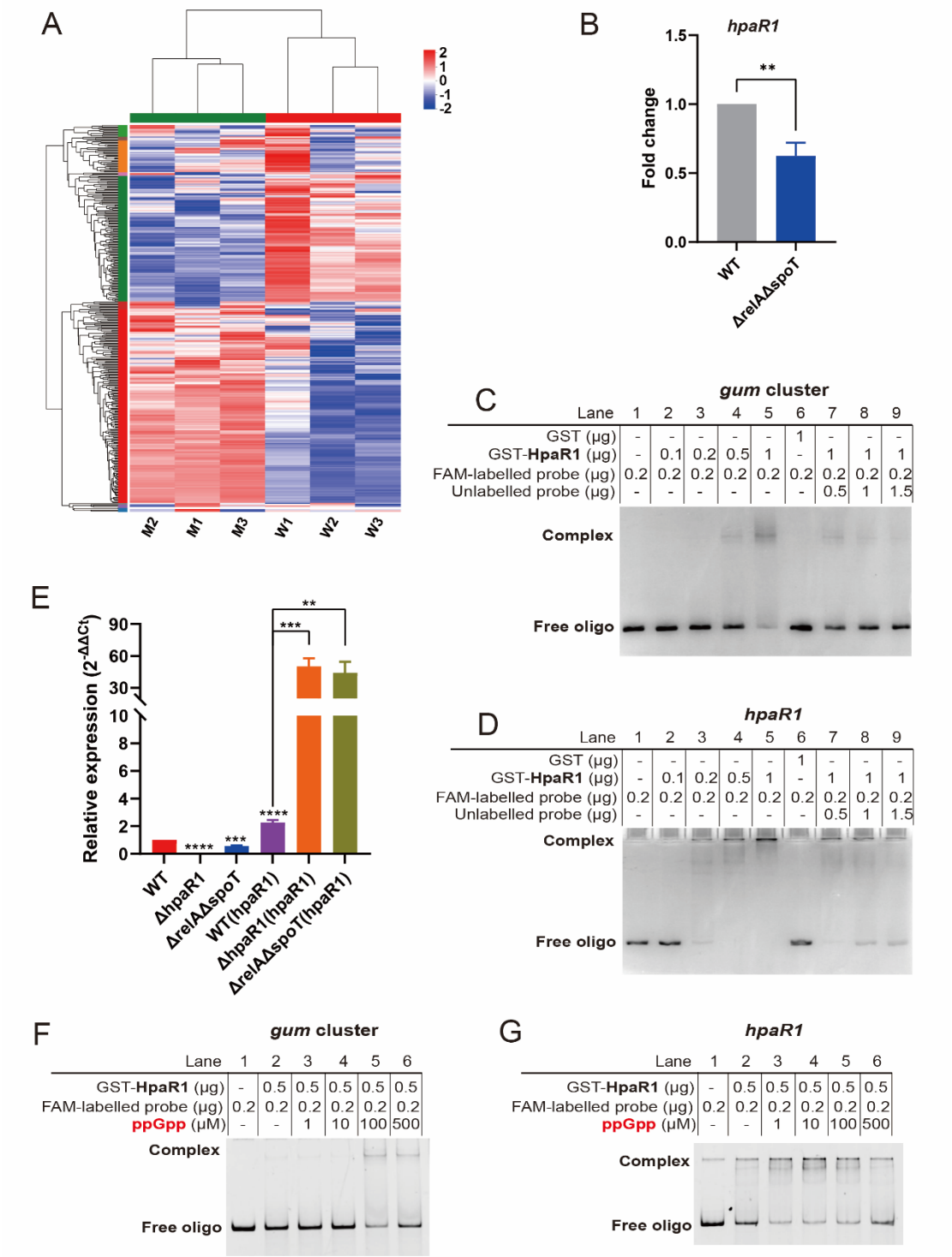

Figure 5 ppGpp regulates the transcription and improves the function of HpaR1 in *Xanthomonas campestris* pv. *campestris*. A, Heat map of 368 predicted transcriptional factor. M indicates double mutant (Δ*relA*Δ*spoT*, ppGpp-deficient mutant), while W indicates wild-type (WT). The numbers 1, 2, and 3 indicate

three independent biological replicates. Expression values are presented as $\log_{10}$(TPM+1) and are row-normalized (Z-score). Blue to red colors reflect gene expression levels (values from -2 to 2). B, The fold change of *hpaR1* for Δ*relA*Δ*spoT* compared to WT in the RNA-seq data. Bars correspond to one standard deviation (SD) from the mean (n = 3), while asterisks indicate significant differences ($P< 0.05$) determined by a one-way ANOVA in conjunction with the Dunnett's multiple comparison test in comparison with WT. **, $P< 0.01$. C, Determination of HpaR1-binding to the promoter region of the *gum* cluster by the electrophoretic mobility shift assay (EMSA). Complex indicates the binding of HpaR1 protein and *gum* promoter, while free oligo indicates unbound *gum* promoter probe. D, Determination of HpaR1-binding to its own promoter region by EMSA. Complex indicates the binding of HpaR1 protein and its own promoter, while free oligo indicates unbound *hpaR1* promoter probe. E, Relative expression of *hpaR1* in the Δ*hpaR1*, Δ*relA*Δ*spoT*, WT(*hpaR1*), Δ*hpaR1*(*hpaR1*), and Δ*relA*Δ*spoT*(*hpaR1*) compared to wild-type (WT). Bars correspond to one standard deviation (SD) from the mean (n = 3). Significant differences ($P< 0.05$) were determined by a one-way ANOVA in conjunction with the Dunnett's multiple comparison test in comparison with WT. Selected pairwise comparisons were further validated using unpaired t tests. **, $P< 0.01$; ***, $P< 0.001$; ****, $P< 0.0001$. F and G, The effect of ppGpp on the binding of HpaR1 to the *gum* promoter (F) and its own promoter (G) was assessed by supplementing the EMSA reaction system with ppGpp. Complex and free oligo indicate the protein-bound and unbound DNA probes, respectively.

HpaR1 enhances EPS production

To evaluate the colony characteristics and EPS production, the strains of WT, Δ*hpaR1*, Δ*relA*Δ*spoT*, WT(*hpaR1*), Δ*hpaR1*(*hpaR1*), and Δ*relA*Δ*spoT*(*hpaR1*) were cultured on the NYGA solid medium

supplemented with 2% glucose. The results revealed that Δ*hpaR1* and Δ*relA*Δ*spoT* colonies exhibited rougher surfaces compared to WT, WT(*hpaR1*), Δ*hpaR1*(*hpaR1*), and Δ*relA*Δ*spoT*(*hpaR1*). Additionally, the colony of Δ*relA*Δ*spoT*(*hpaR1*) manifested an irregular shape (Figure 6A). Moreover, the strains of Δ*relA*Δ*spoT* and Δ*relA*Δ*spoT*(*hpaR1*) produced smaller colonies with colony diameters of 11.54 ± 0.81 mm and 11.58 ± 1.80 mm, respectively, compared to 14.14 ± 0.88 mm, 14.17 ± 1.24 mm, 14.18 ± 0.97 mm, and 14.15 ± 0.80 mm for WT, Δ*hpaR1*, WT(*hpaR1*), and Δ*hpaR1*(*hpaR1*), respectively (Figure 6B).

Notably, although Δ*relA*Δ*spoT*(*hpaR1*) colonies exhibited a reduced diameter, their height was comparable to those of WT(*hpaR1*) and Δ*hpaR1*(*hpaR1*), and greater than that of Δ*relA*Δ*spoT* (Figure 6C), indicating that colony diameter alone is an insufficient parameter for evaluating EPS production. EPS was extracted by absolute ethanol precipitation and quantified, revealing significantly lower yields in Δ*hpaR1* and Δ*relA*Δ*spoT* compared to the WT. In the strains of complementation or overexpression of *hpaR1*, including WT(*hpaR1*), Δ*hpaR1*(*hpaR1*), and Δ*relA*Δ*spoT*(*hpaR1*), the EPS yield reached 13.40 ± 1.20 mg, 8.77 ± 0.74 mg and 6.00 ± 0.56 mg, respectively. These values were significantly higher than those of their corresponding strains without *hpaR1* expression of WT (9.33 ± 0.57 mg), Δ*hpaR1* (5.90 ± 0.50 mg), and Δ*relA*Δ*spoT* (2.23 ± 1.89 mg), respectively (Figure 6D). These findings suggested that HpaR1 enhanced the production of EPS in Xcc.

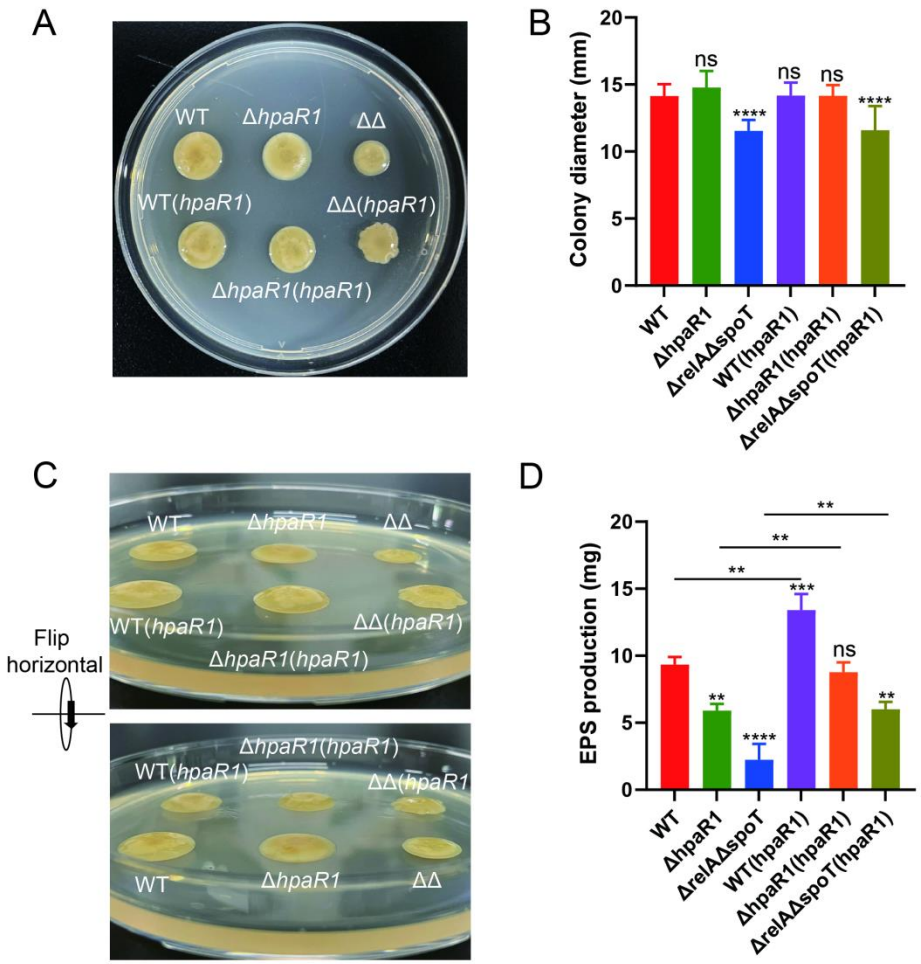

Figure 6 HpaR1 enhances the EPS production. A, The colonies of WT, Δ*hpaR1*, Δ*relA*Δ*spoT*, WT(*hpaR1*), Δ*hpaR1*(*hpaR1*), and Δ*relA*Δ*spoT*(*hpaR1*) were produced during the EPS secretion assay on NYGA containing 2% glucose. ΔΔ indicates Δ*relA*Δ*spoT*, while WT indicates wild-type. B, The colony diameter data were from the EPS assay. Bars correspond to one standard deviation (SD) from the mean (n = 3), while asterisks indicate significant differences ($P < 0.05$) determined by a one-way ANOVA in conjunction with the Dunnett's multiple comparison test in comparison with WT. ****, $P < 0.0001$; ns, no significant differences. C, The height of colony. The two pictures are mirror images of each other. ΔΔ indicates Δ*relA*Δ*spoT*. D, The EPS yield was determined by absolute ethanol deposition method. Bars correspond to one standard deviation (SD) from the mean (n = 3).

Significant differences ($P< 0.05$) were determined by a one-way ANOVA in conjunction with the Dunnett's multiple comparison test in comparison with WT. Selected pairwise comparisons were further validated using unpaired t tests. **, $P< 0.01$; ***, $P< 0.001$; ****, $P< 0.0001$; ns, no significant differences.

Discussion

EPS is an important component of biofilm, providing structural integrity and protective features to the bacterial cell[1]. It is well known that ppGpp regulates biofilm formation[33-37]. Here, ppGpp also could influence EPS production. The ppGpp-deficient mutant exhibited a significantly reduced EPS yield, as quantified by both colony diameter measurement and absolute ethanol precipitation (Figure 1). This result was consistent with our previous report[28]. Similarly, the Δ*relA*(*relA*) complementation strain did not restore EPS production (Figure 1), also aligning with our earlier findings[28]. Furthermore, reintroduction of *relA* failed to recover biofilm formation, extracellular enzyme secretion, swarming motility, or pathogenicity[28]. Although previous transcriptional data indicated strong upregulation of *relA*, the lack of functional recovery suggested that translation-related elements might be compromised when using a shuttle plasmid for complementation. This might explain why *relA* was unable to fully regain its function in this genetic background. This study presented the first comprehensive analysis of both primary and advanced EPS structures in *Xanthomonas campestris* pv. *campestris* (Xcc) using FTIR and SEM. The SEM results showed that spherical lump of Δ*relA*Δ*spoT* was larger than that of WT (Figure 2B) and we speculated that expression of polymerization related genes was down-regulated in ppGpp-deficient mutant, which was consistent with the reduced expression of *gum* expression responsible for assembly, polymerization and secretion of EPS (Figure 3B and 4B).

In *Pseudomonas aeruginosa* and many other bacteria, the second messenger c-di-GMP derives biofilm formation by increasing EPS and adhesin production while downregulating flagellar-based motility[45]. It has been demonstrated that both ppGpp and c-di-GMP play a significant role in the composition of bacterial biofilms, exhibiting a positive influence on the process of biofilm formation in Gram-negative and Gram-positive bacteria[35]. A total of 37 proteins involved in the synthesis and degradation of c-di-GMP were identified in the

genome of Xcc 8004[46]. The RNA-seq results of this study identified 35 c-di-GMP metabolism-related genes among the differentially expressed genes, showing that deficiency of ppGpp could influence the expression of these genes (Data S2). ppGpp and c-di-GMP are structurally similar purine-derived second messengers that appear to exhibit functional overlap in bacterial signaling systems. Previous study showed that an inverse interplay between c-di-GMP and ppGpp directed developmental switches in alphaproteobacteria by targeting DNA replication initiation and cytokinesis through the tubulin FtsZ[47]. Further evidence of their interplay came from *Caulobacter crescentus*, where the small-molecule-binding protein SmbA competitively interacted with both ppGpp and c-di-GMP to regulate metabolic processes including glucose consumption, growth control, and redox balance modulation[48]. The precise molecular mechanisms underlying the interplay between these two global signaling molecules in biofilm regulation, particularly their coordinated control of EPS biosynthesis and matrix assembly, remain to be fully elucidated at both molecular and cellular levels. While ppGpp is known to interact with other nucleotide second messengers (ppApp and c-di-AMP) through various mechanisms including signal conversion, allosteric regulation, and target competition[49], its potential coordination with these molecules in EPS regulation requires further investigation.

It has been revealed that ppGpp has the capacity to regulate transcription in both a direct and indirect manner[26]. Our results illustrated that the *gum* cluster was the crucial factor and ppGpp played a role upstream of the *gum* cluster. RNA-seq results showed that ppGpp could influence transcription and it could facilitate the expression of *hpaR1* (Figure 5A and B). HpaR1 has been shown to repress its own transcription level through binding to its promoter sequence, indicating an autoregulatory feedback inhibition mechanism for HpaR1 expression[44]. This finding is consistent with the results of the present study, which demonstrated that *hpaR1* expression in WT(*hpaR1*) was lower than that in Δ*hpaR1*(*hpaR1*) and Δ*relA*Δ*spoT*(*hpaR1*) (Figure 5E). HpaR1

also could bind to the promoter of the *gum* cluster and positively regulate the expression of *gum* and EPS production (Figure 5C and 6), which was consistent with the previous report that HpaR1-binding could enhance the RNAP-binding to the *gum* promoter, leading to a higher level of transcription[19]. Our results showed ppGpp could enhance the DNA-binding activity of HpaR1. Intriguingly, the enhancing effect of ppGpp on HpaR1 function diminished with increasing ppGpp concentrations (Figure 5F and G). We hypothesize that supraoptimal ppGpp levels may induce conformational changes or steric hindrance within the HpaR1 protein structure, thereby attenuating its functional enhancement.

HpaR1 contains the Pfam00392 (GntR) domain, and its protein structure was predicted using AlphaFold2 (Figure S3A). A Pfam00392 domain was identified in all transcription factors predicted by RNA-seq with differentially expressed genes. This domain was found in 10 additional proteins (XC_RS24700, XC_RS03780, XC_RS18015, XC_RS17360, XC_RS03925, XC_RS13340, XC_RS13345, XC_RS23045, XC_RS02935, and XC_RS12715). These proteins were used to predict their structure (Figure S3B). A comparison of their structures with those of HpaR1 was conducted, and the results of RMSD analysis showed that XC_RS24700, XC_RS03780, XC_RS18015, XC_RS17360, and XC_RS13340 exhibited the greatest similarity (Figure S3C). Given that *hpaR1* was found to be down-regulated in the ppGpp-deficient mutant, it is conceivable that the similarly regulated XC_RS24700, XC_RS03780, XC_RS18015, and XC_RS17360 genes may also perform analogous functions to those of *hpaR1*. Further exploration is warranted to elucidate the precise nature of these relationships.

In conclusion, our study established that ppGpp, HpaR1, and the *gum* cluster collectively regulated EPS production in *Xanthomonas campestris* pv. *campestris* (Xcc). Mechanistically, ppGpp up-regulated *hpaR1* expression, improved the DNA-binding activity of HpaR1, and thereby enhanced the *gum* cluster transcription, leading to increased EPS yield. This novel insight into the ppGpp-HpaR1-*gum* regulatory axis and its role in

EPS production in Xcc may have broader implications for understanding biofilm matrix formation in other microbial systems.

Methods

Bacterial strains, plasmids and culture conditions

The bacterial strains and plasmids used in the current study have been listed in Table 1. The parental isolate *Xanthomonas campestris* pv. *campestris* (Xcc) strain 8004[50], and derived mutants were routinely cultured in Luria-Bertani (LB) broth (5 g/L yeast extract, 5 g/L NaCl and 10 g/L tryptone) or NYG broth (3 g/L yeast extract, 5 g/L hipolypeptone and 20 g/L glycerol) at 28°C with shaking (120 rpm) for 12 h. *Escherichia coli* isolates were cultured in LB broth at 37°C with shaking (200 rpm). When required, solid media was prepared by the addition of 12.8 g/L agar, and selective antibiotics added at the following concentrations: rifampicin, 50 μg/mL; kanamycin, 50 μg/mL; chloramphenicol, 20 μg/mL; tetracycline, 5 μg/mL for Xcc, and 15 μg/mL for *E. coli*; and ampicillin, 100 μg/mL.

Table 1 Bacterial strains and plasmids used in the current study

Strains and plasmids	Properties	Source
Bacterial strains		
8004	*Xanthomonas campestris* pv. *campestris* wild-type isolate, Rif^R	[50]
Δ*relA*	Xcc 8004 *relA* deletion mutant, Rif^R	[28]
Δ*relA*Δ*spoT*	Xcc 8004 *relA* and *spoT* double deletion, ppGpp-deficient mutant, Rif^R	[28]
Δ*relA*(*relA*)	Complementation isolate: Δ*relA* containing pLAFR3*relA*, Rif^R, Tc^R	[28]
Δ*relA*Δ*spoT*(*relA*)	Complementation isolate: Δ*relA*Δ*spoT* containing pLAFR3*relA*, Rif^R, Tc^R	[28]
Δ*relA*Δ*spoT*(*spoT*)	Complementation isolate: Δ*relA*Δ*spoT* containing pLAFR3*spoT*, Rif^R, Tc^R	[28]
pL3-WT	Control isolate: Xcc 8004 containing pLAFR3, Rif^R, Tc^R	[28]
pL3-Δ*relA*	Complementation control isolate: Δ*relA* containing pLAFR3, Rif^R, Tc^R	[28]
pL3-Δ*relA*Δ*spoT*	Complementation control isolate: Δ*relA*Δ*spoT* containing pLAFR3, Rif^R, Tc^R	[28]
Δ*gumD*	Xcc 8004 *gumD* deletion mutant, Rif^R	This study
Δ*relA*Δ*spoT*Δ*gumD*	Xcc 8004 *relA*, *spoT* and *gumD* triple deletion, Rif^R	This study
Δ*gumD*(*gumD*)	Complementation isolate: Δ*gumD* containing pLAFR3*gumD*, Rif^R, Tc^R	This study
Δ*relA*Δ*spoT*Δ*gumD*(*gumD*)	Complementation isolate: Δ*relA*Δ*spoT*Δ*gumD*	This study

	containing pLAFR3*gumD*, Rif^R, Tc^R	
Δ*hpaR1*	Xcc 8004 *hpaR1* deletion mutant, Rif^R	This study
WT(*hpaR1*)	Complementation isolate: Xcc 8004 containing pLAFR3*hpaR1*, Rif^R, Tc^R	This study
Δ*hpaR1*(*hpaR1*)	Complementation isolate: Δ*hpaR1* containing pLAFR3*hpaR1*, Rif^R, Tc^R	This study
Δ*relA*Δ*spoT*(*hpaR1*)	Complementation isolate: Δ*relA*Δ*spoT* containing pLAFR3*hpaR1*, Rif^R, Tc^R	This study
Plasmids		
p2P24Km	Suicide vector for in-frame deletion, derived from pEx18-KCL containing SacB selectable marker; Km^R	[51]
p2P24Km*gumD*	p2P24Km containing *gumD* fragment, Km^R	This study
p2P24Km*hpaR1*	p2P24Km containing *hpaR1* fragment, Km^R	This study
pRK600	Helper plasmid for triparental mating ColE1 *oriV*; RP4; tra+; RP4 *oriT*; Cm^R	[52]
pLAFR3	Xcc expression vector containing RK2 replicon, Tc^R	[54]
pLAFR3*gumD*	Complementation vector: pLAFR3 containing *gumD* gene, Tc^R	This study
pLAFR3*hpaR1*	Complementation vector: pLAFR3 containing *hpaR1* gene, Tc^R	This study
pGEX-GST-HpaR1	pGEX-GST containing *hpaR1* fragment, Amp^R	This study

Rif^R, Km^R, Cm^R, Tc^R, and Amp^R indicate resistance to rifampicin, kanamycin, chloramphenicol, tetracycline, and ampicillin, respectively.

Construction of knock-out mutants

The Δ*gumD* single mutant and Δ*relA*Δ*spoT*Δ*gumD* triple mutant were generated from the parental Xcc 8004 and Δ*relA*Δ*spoT* strain using the triparental mating methods, respectively. Five hundred base pair upstream and downstream fragments of the Xcc *gumD* gene were amplified using the *gumD-Eco*RI-F/*gumD*-del-R and *gumD*-del-F/*gumD-Hin*dIII-R primer sets, respectively, to produce amplification products that contained a fusion sequence compatible with the p2P24Km vector[51]. The resulting PCR fragments were ligated by corresponding primers *gumD-Eco*RI-F/*gumD-Hin*dIII-R using the In-Fusion method, and the resulting fusion products cloned into the p2P24Km vector as restriction fragments (*Eco*RI/*Hin*dIII) to yield the donor vectors p2P24Km*gumD*.

The triparental mating was conducted using *E. coli* donors containing p2P24Km*gumD* plasmid in conjunction with an *E coli* helper strain containing pRK600[52] to transform the Xcc 8004 (WT) or Δ*relA*Δ*spoT* receptor. The mating itself involved mixing 300 μL aliquots of the three strains, which were collected in the log-phase of growth ($OD_{600} \approx 1$), to produce a 900 μL mixture that was subsequently harvested by centrifugation (12000 rpm for 1 min) and washed twice in 300 μL sterilized water before finally being resuspended in 100 μL sterilized water and spread on an NYGA plate. After overnight incubation at 28°C the bacterial mixture from each plate was collected in sterile water and used to prepare 10-fold serial dilutions that were plated on fresh NYGA plates containing rifampicin and kanamycin. After a further 2 days incubation at 28°C individual Xanthomonad-like colonies (yellow in color) were picked and verified by PCR using the Xcc specific primers DLH120/125 detailed in a previous study[53] to confirm that the picked colonies were indeed Xcc. Further PCR using *gumD-Eco*RI-F/*gumD-Hin*dIII-R primer set was conducted to verify that the colonies had been successfully transformed. Colonies with the expected amplicon profile were then subjected to a second round of screening on NYGA containing 8% sucrose supplemented with rifampicin or both rifampicin and kanamycin. Transformants exhibiting growth in the presence of rifampicin but not kanamycin were selected and subsequently confirmed by PCR as described above. All the primers used in the cloning and verification process have been listed in Table S2.

For Δ*hpaR1* mutant construction, the operation step was as described above and the primer sets were *hpaR1*-up-F/*hpaR1*-up-R, *hpaR1*-down-F/*hpaR1*-down-R and *hpaR1*-del-F/*hpaR1*-del-R. All the primers used in the cloning and verification process have been listed in Table S2.

Mutant complementation

Complementation strains reintroducing functional *gumD* gene to the deletion mutants were also generated

by triparental mating. In this case, the full-length genes including the native promoter were amplified using the *gumD-Bam*HI-F3/*gumD-Hin*dIII-R3 primer set (Table S2), and cloned into the pLAFR3[54] vector to yield the plasmid pLAFR3*gumD*. The resulting *E. coli* transformants were then used as the donor strains in the protocol outlined above in conjunction with Δ*gumD* and Δ*relA*Δ*spoT*Δ*gumD* receptor strains.

For the construction of *hpaR1* complementation strain, the operation steps were as described above and the primer set was *hpaR1*-com-F/*hpaR1*-com-R (Table S2).

EPS production assay

The production of exopolysaccharides (EPS) was investigated using NYGA amended with 2% glucose as described in a previous study[13]. Two microliter aliquots of each Xcc suspension (OD_{600} = 0.3) were carefully pipetted onto separate plates and incubated at 28°C for 3 days. Subsequently, Xcc was cultured under light for 4 d. The size and morphology of the resulting colonies were further assessed. A positive correlation was observed between colony diameter and EPS production levels[55].

The yield of EPS was also investigated by absolute ethanol deposition method. For *gum* mutants, one milliliter of Xcc suspension (OD_{600} = 0.3) was carefully inoculated into NYGB liquid medium amended with 4% glucose and the bacteria solution was adjusted to OD_{600} = 1.0 after 1 d of shaking at 28°C. For detection of EPS production of *hpaR1* mutants, the colonies were scraped from NYGA solid medium containing 4% glucose into 0.85% NaCl solution and the bacteria solution was adjusted to OD_{600} = 1.0. The bacteria solution (OD_{600} = 1.0) above were both centrifuged at 8000 rpm for 15 min and the supernatant was collected. The 10 mL of supernatant was slightly pipetted into 20 mL of absolute ethanol. The precipitates were collected after further overnight precipitation at -20°C, centrifugation at 10000 rpm for 15 min, and removal of supernatant. The subsequent samples were freeze-dried at -60°C using a lyophilizer (SCIENTZ-10N, China) for further analysis.

Testing of EPS by Fourier transform infrared spectrometry (FTIR)

The freeze-dried samples of EPS were dissolved in ddH_2O and the FTIR spectrometer (PerkinElmer UATR Two, USA) was used for the detection of functional groups of EPS.

Observation of EPS by scanning electron microscope (SEM)

The freeze-dried samples of EPS were used for morphological analysis. The EPS were coated by sputter (MC1000, HITACHI, Japan) for 20 s and then the coated cells were viewed at 3 kV with SEM (SU8020, HITACHI, Japan).

RNA extraction and quantitative real-time PCR (qPCR) analysis

The different mutant strains of the *gum* cluster (*gumB-gumM*) and *hpaR1* during log-phase growth (OD_{600} = 1.0) were harvested by centrifugation at 12000 rpm for 3 min at 4°C and total RNA extracted using the SV Total RNA Isolation System (Promega Corporation, Beijing, China) according to the protocol of the manufacturer. The detailed steps of qPCR were as followed with our previous study[56]. The standard curve was generated using 4-fold dilutions of the template cDNA, and the PCR efficiency (E) calculated using a linear regression model: $E\ (\%) = (10^{-1/slope}-1) \times 100\%$[57]. The $2^{-\Delta\Delta Ct}$ method was used to calculate the relative expression level of the target genes[58] and the Ct (cycle threshold) values of each gene were normalized to Ct values of the housekeeping genes *ugpC* and *pbpA*[59]. Each treatment was represented by three biological replicates and entire experiment conducted three times. All the primers used for qPCR analysis have been listed in Table S3.

Library construction, data processing and transcriptome analysis

WT and Δ*relA*Δ*spoT* were cultured in NYGB liquid medium amended with 4% glucose. The RNA of WT and Δ*relA*Δ*spoT* was extracted as described above. The RNA library construction and sequencing itself was performed commercially by Shanghai Majorbio Bio-pharm Technology Co., Ltd (Shanghai, China). The

Xanthomonas campestris pv. *campestris* 8004 genome database (RefSeq assembly: GCF_000012105.1) was the reference. Homology searches of the resulting high-quality sequences were performed with major public databases, including NCBI nucleotide (NT) database, Non-Redundant (NR) database, Swiss-Prot database, Pfam database, Cluster of Orthologous Groups (COG) database (http://www.ncbi.nlm.nih.gov), Gene Ontology (GO) database (http://amigo.geneontology.org/amigo), Kyoto Encyclopedia of Genes and Genomes (KEGG) database (http://www.genome.jp/kegg/), and the Search Tool for the Retrieval of Interacting Genes (http://string-db.org/) to ascribe functional annotation.

The expression of genes was normalized as transcrips per million (TPM) values using RSEM software (http://deweylab.biostat.wisc.edu/rsem)[60]. Differentially expressed genes between WT and Δ*relA*Δ*spoT* were analyzed using EdgeR (http://www.bioconductor.org/packages/2.12/bioc/htmL/edgeR.htmL)[61]. For the heatmap generation, hierarchical clustering was performed using the Euclidean distance. To ensure biologically meaningful gene groupings resistant to outliers, average linkage was used for clustering genes (rows). For samples (columns) clustering, complete linkage was employed to achieve well-separated, homogeneous clusters that clearly distinguish between biological conditions. The visualization was generated using the Majorbio Cloud (www.majorbio.com)[62].

Electrophoretic mobility shift assay (EMSA)

The amplified DNA fragment of *hpaR1* was cloned into the expression vector pGEX-GST to generate the recombinant plasmid pGEX-GST-HpaR1 which was transformed into *E. coli* BL21(DE3). For purification of HpaR1 protein, the strain was inducted by 0.5 mM IPTG and HpaR1 protein was purified by anti-GST magnetic beads. The purified protein was mixed with a 470 bp DNA fragment of *hpaR1* and 237 bp DNA fragment of *gum* were amplified by PCR using FAM-labeled and unlabeled primer sets P2736F/P2736R[44] and Pgum2-F/Pgum2-

R, respectively, containing the promoter region of *hpaR1* and *gum* cluster. The mixture was incubated in the buffer (10 mM Tris-HCl, 50 mM KCl, 1 mM DTT, 10% glycerol and 10 mM $MgCl_2$, pH 7.5) containing 1 μg of salmon sperm DNA. When required, ppGpp was added. The samples were loaded onto a 5% non-denatured polyacrylamide gel and visualized after electrophoresis. All the primers used for electrophoretic mobility shift assay have been listed in Table S4.

Statistical analysis

Colony diameter and EPS production in ppGpp mutants and *gum* mutants were analyzed by one-way ANOVA (DPS software) with Duncan's multiple range test ($P < 0.05$). For *hpaR1* mutants, colony diameter, EPS production, and *hpaR1* expression were evaluated by one-way ANOVA in GraphPad Prism 9, followed by Dunnett's test for multiple comparisons ($P < 0.05$). Selected pairwise differences were further confirmed with unpaired t tests. The relative expression of the *gum* cluster in WT, Δ*relA*, and Δ*relA*Δ*spoT* strains was assessed using two-way ANOVA (GraphPad Prism 9) in comparison to the WT sample.

Ethics approval and consent to participate

This article does not contain any studies with animals or humans performed by any of the authors. This study complies with institutional, national and international guidelines and legislation.

Data availability

The RNA-seq raw data of this study has been deposited in the Sequence Read Archive (SRA) database under accession number PRJNA1011498 (https://www.ncbi.nlm.nih.gov/bioproject/ PRJNA1011498).

Acknowledgements

This work was supported by the Natural Science Foundation of Henan Province (number 252300423649) and the Beijing Municipal Natural Science Foundation (number 6222025).

Author contributions

K.B. conceived and designed the research, performed the experiments, analyzed and interpreted the data, and wrote the manuscript. X.X. performed the experiments, analyzed and interpreted the data, and wrote the manuscript. C.Y. and H.Y. helped carry out the experiments. M.L. analyzed the data. N.J. and J.L. designed the research. J.Z. and Z.W. revised the manuscript. L.L. conceived and designed the research and revised the manuscript. All authors read and approved the final manuscript.

Competing interests

The authors declare that they have no conflict of interest.

References

1 Kaur, N. & Dey, P. Bacterial exopolysaccharides as emerging bioactive macromolecules: from fundamentals to applications. *Res. Microbiol.* **174**, 104024 (2023).

2 Bagnol, R., Grijpma, D., Eglin, D. & Moriarty, T. F. The production and application of bacterial exopolysaccharides as biomaterials for bone regeneration. *Carbohyd. Polym.* **291**, 119550 (2022).

3 Pammel, L. H. Bacteriosis of rutabaga (*Bacillus campestris* n. sp.). *Iowa State Coll. Agric. Exp. Stn. Bull.* **27**, 130-134 (1894).

4 Williams, P. H. Black rot: A continuing threat to the world crucifers. *Plant Dis.* **64**, 736-742 (1980).

5 Alvarez, A. M. Black rot of crucifers. in *Mechanisms of Resistance to Plant Diseases* (eds A. J. Slusarenko, R. S. S. Fraser, & L. C. van Loon) 21-52 (Springer Netherlands, 2000).

6 Qiu, J. & He, Y. Advances in applications and research of xanthan gum. *Acta Laser Biol. Sinica* **28**, 385-393, 409 (2019).

7 Yun, M. H. et al. Xanthan induces plant susceptibility by suppressing callose deposition. *Plant Physiol.* **141**, 178-187 (2006).

8 Kakkar, A., Nizampatnam, N. R., Kondreddy, A., Pradhan, B. B. & Chatterjee, S. *Xanthomonas campestris* cell–cell signaling molecule DSF (diffusible signal factor) elicits innate immunity in plants and is suppressed by the exopolysaccharide xanthan. *J. Exp. Bot.* **66**, 6697-6714 (2015).

9 Ielpi, L., Couso, R. O. & Dankert, M. A. Sequential assembly and polymerization of the polyprenol-linked pentasaccharide repeating unit of the xanthan polysaccharide in *Xanthomonas campestris*. *J. Bacteriol.* **175**, 2490-2500 (1993).

10 Katzen, F., Becker, A., Zorreguieta, A., Pühler, A. & Ielpi, L. Promoter analysis of the *Xanthomonas campestris* pv. *campestris gum* operon directing biosynthesis of the xanthan polysaccharide. *J. Bacteriol.* **178**, 4313-4318 (1996).

11 Galván, E. M. *et al.* Xanthan chain length is modulated by increasing the availability of the polysaccharide copolymerase protein GumC and the outer membrane polysaccharide export protein GumB. *Glycobiology* **23**, 259-272 (2013).

12 Katzen, F. *et al. Xanthomonas campestris* pv. *campestris gum* mutants: Effects on xanthan biosynthesis and plant virulence. *J. Bacteriol.* **180**, 1607-1617 (1998).

13 Tang, J. *et al.* Genetic and molecular analysis of a cluster of rpf genes involved in positive regulation of synthesis of extracellular enzymes and polysaccharide in *Xanthomonas campestris* pathovar *campestris*. *Mol. Gen. Genet.* **226**, 409-417 (1991).

14 Slater, H., Alvarez-Morales, A., Barber, C. E., Daniels, M. J. & Dow, J. M. A two-component system involving an HD-GYP domain protein links cell–cell signalling to pathogenicity gene expression in *Xanthomonas campestris*. *Mol. Microbiol.* **38**, 986-1003 (2000).

15 Barber, C. E. *et al.* A novel regulatory system required for pathogenicity of *Xanthomonas campestris* is mediated by a small diffusible signal molecule. *Mol. Microbiol.* **24**, 555-566 (1997).

16 Chin, K.-H. et al. The cAMP receptor-like protein CLP is a novel c-di-GMP receptor linking cell–cell signaling to virulence gene expression in *Xanthomonas campestris*. *J. Mol. Biol.* **396**, 646-662 (2010).

17 Tao, F., He, Y.-W., Wu, D.-H., Swarup, S. & Zhang, L.-H. The cyclic nucleotide monophosphate domain of *Xanthomonas campestris* global regulator Clp defines a new class of cyclic di-GMP effectors. *J. Bacteriol.*

192, 1020-1029 (2010).

18 de Crecy-Lagard, V. et al. A *Xanthomonas campestris* pv. *campestris* protein similar to catabolite activation factor is involved in regulation of phytopathogenicity. *J. Bacteriol.* **172**, 5877-5883 (1990).

19 Su, H.-Z. *et al.* Characterization of the GntR family regulator HpaR1 of the crucifer black rot pathogen *Xanthomonas campestris* pathovar *campestris*. *Sci. Rep.* **6**, 19862 (2016).

20 Atkinson, G. C., Tenson, T. & Hauryliuk, V. The RelA/SpoT homolog (RSH) superfamily: distribution and functional evolution of ppGpp synthetases and hydrolases across the tree of life. *PLoS One* **6**, e23479 (2011).

21 Hauryliuk, V., Atkinson, G. C., Murakami, K. S., Tenson, T. & Gerdes, K. Recent functional insights into the role of (p)ppGpp in bacterial physiology. *Nat. Rev. Microbiol.* **13**, 298-309 (2015).

22 Irving, S. E., Choudhury, N. R. & Corrigan, R. M. The stringent response and physiological roles of (pp)pGpp in bacteria. *Nat. Rev. Microbiol.* **19**, 256-271 (2021).

23 Ronneau, S. & Hallez, R. Make and break the alarmone: regulation of (p)ppGpp synthetase/hydrolase enzymes in bacteria. *FEMS Microbiol. Rev.* **43**, 389-400 (2019).

24 Xiao, H. *et al.* Residual guanosine 3',5'-bispyrophosphate synthetic activityof *relA* null mutants can be eliminated by spoT null mutations. *J. Biol. Chem.* **266**, 5980-5990 (1991).

25 Srivatsan, A. & Wang, J. D. Control of bacterial transcription, translation and replication by (p)ppGpp. *Curr. Opin. Microbiol.* **11**, 100-105 (2008).

26 Liu, K., Bittner, A. N. & Wang, J. D. Diversity in (p)ppGpp metabolism and effectors. *Curr. Opin. Microbiol.* **24**, 72-79 (2015).

27 Bai, K. *et al.* RNA-Seq analysis discovers the critical role of Rel in ppGpp synthesis, pathogenicity, and the VBNC state of *Clavibacter michiganensis*. *Phytopathology*, **112**, 1844-1858 (2022).

28 Bai, K. *et al.* The role of RelA and SpoT on ppGpp production, stress response, growth regulation and pathogenicity in *Xanthomonas campestris* pv. *campestris*. *Microbiol. Spectr.* **9**, e02057-02021 (2021).

29 Wang, J., Gardiol, N., Burr, T., Salmond, G. P. & Welch, M. RelA-dependent (p)ppGpp production controls exoenzyme synthesis in *Erwinia carotovora* subsp. *atroseptica*. *J. Bacteriol.* **189**, 7643-7652 (2007).

30 Yang, H. W., Yu, M., Lee, J. H., Chatnaparat, T. & Zhao, Y. The stringent response regulator (p) ppGpp mediates virulence gene expression and survival in *Erwinia amylovora*. *BMC Genomics* **21**, 261 (2020).

31 Zhang, Y., Teper, D., Xu, J. & Wang, N. Stringent response regulators (p)ppGpp and DksA positively regulate virulence and host adaptation of *Xanthomonas citri*. *Mol. Plant Pathol.* **20**, 1550-1565 (2019).

32 Xu, X. *et al.* Bacterial alarmone (p)ppGpp mediates the pathogenicity of *Clavibacter michiganensis* via a dual mechanism that affects both enzyme production and the Tat secretion system. *mSystems*, e0013525 (2025).

33 Lemos, J. A. C., Brown, T. A. & Burne, R. A. Effects of RelA on key virulence properties of planktonic and biofilm populations of *Streptococcus mutans*. *Infect. Immu.* **72**, 1431-1440 (2004).

34 Ge, X. *et al.* Bifunctional enzyme SpoT is involved in biofilm formation of *Helicobacter pylori* with multidrug resistance by upregulating efflux pump Hp1174 (*gluP*). *Antimicrob. Agents Ch.* **62**, e00957-18 (2018).

35 Gupta, K. R., Kasetty, S. & Chatterji, D. Novel functions of (p)ppGpp and Cyclic di-GMP in mycobacterial physiology revealed by phenotype microarray analysis of wild-type and isogenic strains of *Mycobacterium smegmatis*. *Appl. Environ. Microb.* **81**, 2571-2578 (2015).

36 Nguyen, D. *et al.* Active starvation responses mediate antibiotic tolerance in biofilms and nutrient-limited

bacteria. *Science* **334**, 982-986 (2011).

37 Taylor, C. M. *et al. Listeria monocytogenes relA* and *hpt* mutants are impaired in surface-attached growth and virulence. *J. Bacteriol.* **184**, 621-628 (2002).

38 Li, W., Liu, M., Siddique, M. S., Graham, N. & Yu, W. Contribution of bacterial extracellular polymeric substances (EPS) in surface water purification. *Environ. Pollut.* **280**, 116998 (2021).

39 Guibaud, G., Comte, S., Bordas, F., Dupuy, S. & Baudu, M. Comparison of the complexation potential of extracellular polymeric substances (EPS), extracted from activated sludges and produced by pure bacteria strains, for cadmium, lead and nickel. *Chemosphere* **59**, 629-638 (2005).

40 Liao, B. Q., Allen, D. G., Droppo, I. G., Leppard, G. G. & Liss, S. N. Surface properties of sludge and their role in bioflocculation and settleability. *Water Res.* **35**, 339-350 (2001).

41 Zhang, P. *et al.* Extracellular protein analysis of activated sludge and their functions in wastewater treatment plant by shotgun proteomics. *Sci. Rep.* **5**, 12041 (2015).

42 Pandian, V., Babinastarlin, S., Shankar, T., Sivakumar, T. & Kasirajan, A. Quantification and characterization of exopolysaccharides from *Bacillus subtilis* (MTCC 121). *Adv. Biol. Res.* **5**, 71-76 (2011).

43 Vinothkanna, A. *et al.* Structural characterization, functional and biological activities of an exopolysaccharide produced by probiotic *Bacillus licheniformis* AG-06 from Indian polyherbal fermented traditional medicine. *Int. J. Biol. Macromol.* **174**, 144-152 (2021).

44 An, S.-Q. *et al.* Systematic mutagenesis of all predicted *gntR* genes in *Xanthomonas campestris* pv. *campestris* reveals a GntR family transcriptional regulator controlling hypersensitive response and virulence. *Mol. Plant Microbe In.* **24**, 1027-1039 (2011).

45 Valentini, M. & Filloux, A. Biofilms and Cyclic di-GMP (c-di-GMP) Signaling: Lessons from *Pseudomonas aeruginosa* and other bacteria. *J. Biol. Chem.* **291**, 12547-12555 (2016).

46 Ryan, R. P. *et al.* Cyclic di-GMP signalling in the virulence and environmental adaptation of *Xanthomonas campestris*. *Mol. Microbiol.* **63**, 429-442 (2006).

47 Hallez, R., Delaby, M., Sanselicio, S. & Viollier, P. H. Hit the right spots: cell cycle control by phosphorylated guanosines in alphaproteobacteria. *Nat. Rev. Microbiol.* **15**, 137-148 (2017).

48 Shyp, V. *et al.* Reciprocal growth control by competitive binding of nucleotide second messengers to a metabolic switch in *Caulobacter crescentus*. *Nat. Microbiol.* **6**, 59-72 (2021).

49 Fung, D. K., Trinquier, A. E. & Wang, J. D. Crosstalk between (p)ppGpp and other nucleotide second messengers. *Curr. Opin. Microbiol.* **76**, 102398 (2023).

50 Turner, P., Barber, C. & Daniels, M. Behaviour of the transposons Tn5 and Tn7 in *Xanthomonas campestris* pv. *campestris*. *Mol. Gen. Genet.* **195**, 101-107 (1984).

51 Zhang, Y., Zhang, Y., Zhang, B., Wu, X. & Zhang, L. Q. Effect of carbon sources on production of 2,4-diacetylphloroglucinol in *Pseudomonas fluorescens* 2P24. *Acta Microbiol. Sin.* **58**, 1202-1212 (2018).

52 Kessler, B., de Lorenzo, V. & Timmis, K. N. A general system to integrate *lacZ* fusions into the chromosomes of gram-negative eubacteria: regulation of the Pm promoter of the Tol plasmid studied with all controlling elements in monocopy. *Mol. Gen. Genet.* **233**, 293-301 (1992).

53 Berg, T., Tesoriero, L. & Hailstones, D. L. PCR-based detection of *Xanthomonas campestris* pathovars in *Brassica* seed. *Plant Pathol.* **54**, 416-427 (2005).

54 Staskawicz, B., Dahlbeck, D., Keen, N. & Napoli, C. Molecular characterization of cloned avirulence genes from race 0 and race 1 of *Pseudomonas syringae* pv. *glycinea*. *J. Bacteriol.* **169**, 5789-5794 (1987).

55 Osbourn, A. E., Clarke, B. R., Stevens, B. J. H. & Daniels, M. J. Use of oligonucleotide probes to identify members of two-component regulatory systems in *Xanthomonas campestris* pathor *campestris*. *Mol. Gen. Genet.* **222**, 145-151 (1990).

56 Bai, K. *et al.* Transcriptional profiling of *Xanthomonas campestris* pv. *campestris* in viable but nonculturable state. *BMC Genomics* **24**, 105 (2023).

57 Radonic, A. *et al.* Guideline to reference gene selection for quantitative real-time PCR. *Biochem. Bioph. Res. Co.* **313**, 856-862 (2004).

58 Pfaffl, M. W. A new mathematical model for relative quantification in real- time RT-PCR. *Nucleic Acids Res.* **29**, 2002-2007 (2001).

59 Bai, K. *et al.* Evaluation of optimal reference genes for the normalization by qPCR in viable but nonculturable state in *Xanthomonas campestris* pv. *campestris*. *J. Phytopathol.* **170**, 399-407 (2022).

60 Li, B. & Dewey, C. N. RSEM: accurate transcript quantification from RNA-Seq data with or without a reference genome. *BMC Bioinformatics* **12**, 323 (2010).

61 Robinson, M. D., McCarthy, D. J. & Smyth, G. K. edgeR: a Bioconductor package for differential expression analysis of digital gene expression data. *Bioinformatics* **26**, 139-140 (2010).

62 Han, C. *et al.* Majorbio Cloud 2024: Update single-cell and multiomics workflows. *iMeta* **3**, e217 (2024).

Table and Figure legends

Table 1 Bacterial strains and plasmids used in the current study

Rif^R, Km^R, Cm^R, Tc^R, and Amp^R indicate resistance to rifampicin, kanamycin, chloramphenicol, tetracycline, and ampicillin, respectively.

Figure 1 Effect of ppGpp on EPS production. A, The colonies were produced during the EPS secretion assay on NYGA containing 2% glucose. B, The colony diameter data were obtained from the EPS assay. C, EPS yield was determined by absolute ethanol deposition method. Bars correspond to one standard deviation (SD) from the mean (n = 3), while different letters above columns indicate significant differences ($P< 0.05$) among samples in different mutants according to a one-way ANOVA in conjunction with the Duncan's multiple range test.

Figure 2 Effect of ppGpp on EPS characteristics. A, The EPS primary structure of WT, Δ*relA*, Δ*relA*Δ*spoT*, pL3-WT, pL3-Δ*relA*, Δ*relA*(*relA*), pL3-Δ*relA*Δ*spoT*, Δ*relA*Δ*spoT*(*relA*), and Δ*relA*Δ*spoT*(*spoT*) detected by Fourier transform infrared spectrometry (FTIR). The functional groups of EPS were labeled. B, The EPS advanced structure of WT and Δ*relA*Δ*spoT* determined by scanning electron microscope (SEM). Bar indicates 1 μm.

Figure 3 ppGpp regulates *gum* gene cluster expression and EPS production. A, The location on the genome of the *gum* cluster (*gumB- gumM*) in Xcc 8004. B, The gene expression of *gum* cluster in WT and Δ*relA*Δ*spoT*. Bars correspond to one standard deviation (SD) from the mean (n = 3), while asterisks indicate significant differences ($P< 0.05$) determined by a one-way ANOVA in conjunction with the Dunnett's multiple comparison test in comparison with WT. ****, $P< 0.0001$. C, EPS yield of WT, Δ*relA*Δ*spoT*, Δ*gumD*, Δ*relA*Δ*spoT*Δ*gumD*, Δ*gumD*(*gumD*), and Δ*relA*Δ*spoT*Δ*gumD*(*gumD*). Bars correspond to one standard deviation (SD) from the mean (n = 3), while different letters above columns indicate significant differences ($P< 0.05$) among samples in

different mutants according to a one-way ANOVA in conjunction with the Duncan's multiple range test.

Figure 4 Transcriptomic analysis reveals the effect of ppGpp on gene expression levels including the *gum* cluster in *Xanthomonas campestris* pv. *campestris*. A, The heatmap depicting the average expression levels of the 4173 genes identified through RNA-seq alignment to the reference genome (RefSeq assembly: GCF_000012105.1) was generated to visualize the similarity between different treatments. M indicates double mutant (Δ*relA*Δ*spoT,* ppGpp-deficient mutant), while W indicates wild-type (WT). The numbers 1, 2, and 3 indicate three independent biological replicates. Expression values are presented as $\log_{10}$(TPM+1) and are row-normalized (Z-score). Blue to red colors reflect gene expression levels (values from -2 to 2). B, The fold change of the *gum* cluster (*gumB-gumM*) in Δ*relA*Δ*spoT* compared with wild-type (WT). The asterisks indicate significant differences ($P< 0.05$) determined by a one-way ANOVA in conjunction with the Dunnett's multiple comparison test in comparison with WT. **, $P< 0.01$; ***, $P< 0.001$; ****, $P< 0.0001$.

Figure 5 ppGpp regulates the transcription and improves the function of HpaR1 in *Xanthomonas campestris* pv. *campestris*. A, Heat map of 368 predicted transcriptional factor. M indicates double mutant (Δ*relA*Δ*spoT,* ppGpp-deficient mutant), while W indicates wild-type (WT). The numbers 1, 2, and 3 indicate three independent biological replicates. Expression values are presented as $\log_{10}$(TPM+1) and are row-normalized (Z-score). Blue to red colors reflect gene expression levels (values from -2 to 2). B, The fold change of *hpaR1* for Δ*relA*Δ*spoT* compared to WT in the RNA-seq data. Bars correspond to one standard deviation (SD) from the mean (n = 3), while asterisks indicate significant differences ($P< 0.05$) determined by a one-way ANOVA in conjunction with the Dunnett's multiple comparison test in comparison with WT. **, $P< 0.01$. C, Determination of HpaR1-binding to the promoter region of the *gum* cluster by the electrophoretic mobility shift assay (EMSA). Complex indicates the binding of HpaR1 protein and *gum* promoter, while free oligo indicates

unbound *gum* promoter probe. D, Determination of HpaR1-binding to its own promoter region by EMSA. Complex indicates the binding of HpaR1 protein and its own promoter, while free oligo indicates unbound *hpaR1* promoter probe. E, Relative expression of *hpaR1* in the Δ*hpaR1*, Δ*relA*Δ*spoT*, WT(*hpaR1*), Δ*hpaR1*(*hpaR1*), and Δ*relA*Δ*spoT*(*hpaR1*) compared to wild-type (WT). Bars correspond to one standard deviation (SD) from the mean (n = 3). Significant differences ($P< 0.05$) were determined by a one-way ANOVA in conjunction with the Dunnett's multiple comparison test in comparison with WT. Selected pairwise comparisons were further validated using unpaired t tests. **, $P< 0.01$; ***, $P< 0.001$; ****, $P< 0.0001$. F and G, The effect of ppGpp on the binding of HpaR1 to the *gum* promoter (F) and its own promoter (G) was assessed by supplementing the EMSA reaction system with ppGpp. Complex and free oligo indicate the protein-bound and unbound DNA probes, respectively.

Figure 6 HpaR1 enhances the EPS production. A, The colonies of WT, Δ*hpaR1*, Δ*relA*Δ*spoT*, WT(*hpaR1*), Δ*hpaR1*(*hpaR1*), and Δ*relA*Δ*spoT*(*hpaR1*) were produced during the EPS secretion assay on NYGA containing 2% glucose. ΔΔ indicates Δ*relA*Δ*spoT*, while WT indicates wild-type. B, The colony diameter data were from the EPS assay. Bars correspond to one standard deviation (SD) from the mean (n = 3), while asterisks indicate significant differences ($P< 0.05$) determined by a one-way ANOVA in conjunction with the Dunnett's multiple comparison test in comparison with WT. ****, $P< 0.0001$; ns, no significant differences. C, The height of colony. The two pictures are mirror images of each other. ΔΔ indicates Δ*relA*Δ*spoT*. D, The EPS yield was determined by absolute ethanol deposition method. Bars correspond to one standard deviation (SD) from the mean (n = 3). Significant differences ($P< 0.05$) were determined by a one-way ANOVA in conjunction with the Dunnett's multiple comparison test in comparison with WT. Selected pairwise comparisons were further validated using unpaired t tests. **, $P< 0.01$; ***, $P< 0.001$; ****, $P< 0.0001$; ns, no significant differences.